Small-Angle-Scattering Resolved Catanionic Unilamellar Vesicles as Molecule Carriers

Chen-An Wang,[a] Yi-Qi Yeh,[a,*] Chung-Yuan Mou,[b] Chun-Jen Su,[a] Wei-Ru Wu,[a] U-Ser Jeng,[a,c,*]

[a]*National Synchrotron Radiation Research Center, Hsinchu Science Park, Hsinchu 30076, Taiwan*

[b]*Department of Chemistry and Center of Condensed Matter Sciences, National Taiwan University, Taipei 10617, Taiwan*

[c]*Department of Chemical Engineering, National Tsing Hua University, Hsinchu 30013, Taiwan*

*Corresponding Authors

H I G H L I G H T S

- Structure and composition of the catanionic unilamellar vesicles formed in solution of SDS and CTAB are resolved.
- The hydrophobic shell of the vesicle bilayer comprises highly interdigitated catanionic surfactant chains.
- A triblock copolymer could intervene into the vesicle bilayer for enlarged vesicles.
- Our findings suggest a capacity and limits of using catanionic unilamellar vesicles as molecule carriers.

ABSTRACT. Structure and composition of the unilamellar vesicles (ULV) formed with catanionic surfactant of sodium dodecylsulfate (SDS) and cetyltrimethylammonium bromide (CTAB) are revealed using small-angle X-ray and neutron scattering (SAXS and SANS) and freeze-fracture-replication transmission electron microscopy (FFR-TEM). Imaging and scattering results consistently indicate a globular shape of the ULV, having a core size of 48 nm and a bilayer

thickness of 32 Å; the bilayer comprises a central aliphatic shell of 24 Å, sandwiched by two headgroup shells, each of ca. 4 Å thickness. From the zero-angle scattering intensity ratio of the SAXS and SANS data, a SDS/CTAB composition ratio of 3:4 for the ULV bilayer is deduced. Poly(oxyethylene-*b*-oxypropylene-*b*-oxyethylene) (P123), a triblock copolymer, is found to intervene into the ULV bilayer of the catanionic surfactant in solution, leading to successively enlarged complex ULV, as P123 concentration in the solution increases. The ULV of SDS/CTAB is saturated with P123-loading after a critical concertation of 0.067 mM P123; thereafter, formation and proliferation of constant-sized, P123-based core-shell micelles are observed with increase of P123 concentration. A structural model of P123-embedded ULV of the catanionic surfactant is proposed. These results suggest a capacity and limits of using the catanionic ULV as molecule carriers.

KEYWORDS. SAXS and SANS, FFR-TEM, unilamellar vesicles, catanionic surfactant, molecule carrier.

Graphical Abstract.

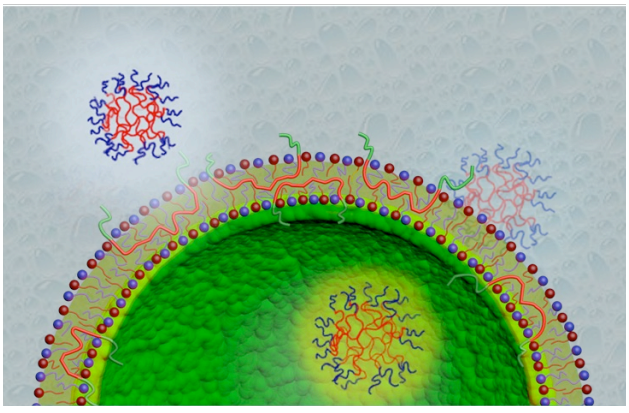

1. Introduction

Catanionic surfactant, comprising cationic and anionic surfactants, forms aggregates in aqueous solution, which are of potential applications as molecular carriers [1-3]. Part of the advantages of using catanionic surfactant aggregates as molecular carriers associate with their tunable aggregation structures of duo-compartmentalization of both hydrophobic and hydrophilic molecules [3]. Surfactant aggregation structures are often manipulated through the packing parameter defined by $p = v/(al)$, where v is the volume of the surfactant hydrophobic tail, a the effective area per headgroup, and l the length of the hydrophobic tail. Surfactants with increasingly higher values of the packing parameter tend to form aggregates of successively reduced interfacial curvatures, ranging from spherical micelles ($p < 1/3$), to cylindrical micelles ($p \sim 1/2$), to vesicles ($1/2 < p < 1$), and to planar bilayers ($p \sim 1$) [4]. Due to tight packing of the oppositely charged headgroups for an effectively lager packing parameter (smaller effective a with similar v values), the catanionic surfactant could form vesicles, in addition to the individual anionic and cationic surfactant micelles [5]. Particularly, tuning the surfactant molar ratio of catanionic surfactant away from equal molar composition facilitates formation of charged and stabilized vesicles in aqueous solution [5-6].

Previous studies [1, 5-7] showed that the sizes of catanionic-surfactant unilamellar vesicles (CS-ULV) comprising cetyltrimethylammonium bromide (CTAB) and sodium dodecylsulfate (SDS) were dependent of the surfactant mixing ratio and temperature [5,6]. The average hydrodynamic diameter of the ULV reduced from 700 nm to 250 nm [6], when the surfactant molar ratio R = [SDS]/[CTAB] in solution increased from 1.1 to 2.4; the vesicle size could reduce from 500 nm at 313 K °C to 150 - 250 nm at a critical temperature near 318 K [2,6]. The drastic reduction in vesicle size with increases of sample temperature and/or solution net charges, is

accompanied inevitably by higher vesicle curvatures that might result from reorganization of the vesicle composition. Previous measurements on surface excess concentration and zeta potential of catanionic surfactant solutions suggested that the corresponding CS-ULV compositions might match that measured from the air-liquid or solid-liquid interfaces [7,8]. However, there was no report available on direct measurements of the composition of CS-ULV in solution. Moreover, despite SDS-based catanionic vesicles were shown to carry and release drug molecules [3], specific location of the cargo molecules inside the CS-ULV remains elusive.

In this study, using combined small-angle X-ray and neutron scattering (SAXS and SANS) [9-11], we resolve both the structure and composition of the catanionic ULV formed in solutions of 20.8 mM SDS and 13.9 mM CTAB (for a molecular ratio R = 1.5) at 318 K. Such a solution composition was optimized for best yield in the synthesis of mesoporous silica nanochannel plates with perpendicular channel orientation [11,12]. This study takes a different direction from the previous nanochannel fabrication, and focuses on the structure-composition of the catanionic ULV formed with SDS/CTAB and its molecule carrying structure with a triblock copolymer.

As in the case of liposomes, catanionic vesicles can be a drug reservoir system for encapsulating active ingredients and therefore protecting them during their targeted delivery in a biological environment for reduced toxicity and improved bioavailability. However, development of catanionic vesicles as drug carriers has been much less, compared to liposome, due to their limited stability when combined with drug molecules under various physiological conditions [12]. In this study, we show that by adding a third nonionic surfactant P123 the unilammellar structure can be tuned to higher rigidity and thus improved stability. Both the structure and stability of the bilayer of the vesicle can be carefully modulated. Our detailed structural study, by SANS and

SAXS, of the P123/CTAB/SDS vesicle would shed lights on understanding the physicochemical interactions involved, and pave ways for drug formulations in future applications.

2. Materials and methods.

2.1. Sample Preparation. Aqueous solutions of 13.7 mM CTAB and 20.6 mM SDS, corresponding a SDS/CTAB molar ratio of R = 1.5, were prepared for formation of unilamellar vesicles at 318 K. Poly(oxyethylene-b-oxyropylene-b-oxyethylene) $EO_{20}PO_{70}EO_{20}$ (P123), of an average molecular mass 5800 Da (polydispersity index ~1.1) and a nearly vanishing critical micelle concentration (CMC) concentration below 0.002 mM at 318 K [13], was mixed into the catanionic surfactant solution for ternary mixtures, with P123 concentrations ranging from 0.04 to 1.6 mM. Parallel SANS sample solutions were prepared using aliphatic-chain-deuterated SDS (d-SDS, 98 atom % D) and CTAB (d-CTAB, 98 atom % D), in D_2O (99.8 atom % D); such deuteration selections would allow better SANS sensitivity to distribution or aggregation of P123 (of a low neuron scattering-length-density, SLD) in the ULV of d-SDS and d-CTAB in D_2O (all of high values of SLD), as illustrated in Fig. 1. All the sample solutions were adjusted to pH 4.5, using sulfuric acid and sodium hydroxide. The acid dissociation constant pKa of D_2O at 318 K is 14.3; furthermore, there is only one oxygen-bound hydrogen (H) out of the 81 H of P123 that would proceed D-H exchange with D_2O in the sample solutions [14], which would contribute to an estimated change of ~ 0.2% in the SLD of P123. Therefore, the minute D-H exchange effect in the sample solutions was neglected. We note that a solvent SLD value of 6.30×10^{-6} Å^{-2} was used in the data fitting, which was calculated based on the deuteration and density of D_2O at 318 K [11].

2.2. Freeze-fracture replication TEM

Freeze-fracture replication TEM was performed with a Balzers freeze-fracture apparatus (BAF 400 D), following the details reported previously [11]. Briefly, the liquid sample was submerged into a liquid nitrogen reservoir and transferred into a sample-fracture housing precooled in liquid nitrogen. The frozen sample was then inserted into a vacuum chamber maintained at 168 K for split open into fractures. The fracture surfaces were first shadowed with a 2-nm layer of platinum-carbon, followed by coating with a 20-nm carbon layer, to preserve the structural features of the surfactant aggregates. The replicas retrieved from the thawed samples were cleaned in deionized water, then mounted on copper grids for TEM observation (Hitachi S-7100, 75 keV) at room temperature.

2.3. Small Angle Scattering Measurements

2.3.1. Measurements. SAXS data were collected at 318 K using the 23A SAXS instrument of the Taiwan Light Source (TLS) of the National Synchrotron Radiation Research Center (NSRRC) in Hsinchu [15]. With a beam of 12.0 keV (X-ray wavelength λ = 1.033 Å of 1% dispersion) and a sample-to-detector distance of 3048 mm, SAXS data were collected from samples thermostated at 318 K in a Kapton-sealed sample cell of 2.0 mm X-ray path length, using an area detector MARCCD165. The SAXS patterns were circularly averaged into 1D intensity distribution function $I(q)$, and corrected for transmission, background, and pixel sensitivity of the detector, then scaled to the absolute intensity in units of cm^{-1} via comparing to the absolute scattering intensity of water [15]. The scattering vector $q = 4\pi\lambda^{-1}\sin\theta$ is defined by the scattering angle 2θ and wavelength λ of the radiation quanta. Parallel SANS data were collected using the small-angle scattering

diffractometer at the KWS-1 beamline of FRM II research reactor in Garching, Germany [16]. Neutron wavelength was set $\lambda = 4.5$ Å, with a wavelength spread $\Delta\lambda/\lambda = 15$ %. Three detector distances of 1.7, 7.7, and 19.7 m were used to cover a wide q-range of 0.003 – 0.3 Å^{-1}. Quartz cuvettes of 1 mm path length were mounted on a thermostated sample holder at 318 K. Sample transmission was measured simultaneously with SANS data collection using a beam-monitor embedded inside the beamstop. The data were scaled to the absolute scattering intensity, via the scattering intensity from H_2O at the same instrumental condition. SANS data reductions were performed using the software QtiKWS of the beamline. The SANS instrumental q-resolution was included in the model fitting of the data using the SasView (version 4.2.2) analysis package (http://www.sasview.org/).

2.3.2. Data analysis. The SAXS and SANS intensity profiles are described by

$$I(q) = n_p P(q) S(q) \qquad (1)$$

with the number density n_p [15], the form factor $P(q)$, and the structure factor $S(q)$ of the scattering particles. For CS-ULV of a surfactant bilayer, a spherical core-multi-shell form factor $P(q) = |F(q)|^2$ with

$$F(q) = \sum_{i=0}^{N} V(r_i)(\rho_{i+1} - \rho_i) \frac{3j_1(qr_i)}{qr_i} \qquad (2)$$

was adopted in data analysis (http://www.qtisas.com/compile/sasview/sphere/core-multi-shell). As illustrated in Fig. 1a, $i = 0$ and 4 are respectively for the solvent respectively in the

core and environment of the catanionic surfactant vesicle, whereas i =1, 2, and 3 are for the indexes of the first inner-headgroup shell, second aliphatic-chain shell, and third outer-headgroup shell of the CS-ULV, respectively. The sphere volume $V(r_i)$ is defined by the corresponding core and shell radii r_i; ρ_i is the scattering-length-density of the i^{th} shell, and $j_1(X) = (\sin X - X\cos X)/X^2$ with $X_i = qr_i$ is the spherical Bessel function of the first order [16]. For charged vesicles, the structure factor is approximated by the rescaled-mean-spherical-approximation (RMSA) $S(q)$ in the fitting process [17-18], assuming rigid charged spheres interacting through a screened Coulomb potential of an effective hard-sphere diameter σ. The joint fitting of SAXS and SANS data sets for consistent structural parameters was done using the protocol of the SasView (version 4.2.2) analysis package.

At q = 0, Eq. (1) reduces to the forward scattering intensity I_o of the CS-ULV

$$I_o = n_p[N_s\Delta\rho_s V_s + N_{ct}\Delta\rho_{ct}V_{ct}]^2 \qquad (3)$$

which depends on the CS-ULV aggregation number comprising N_s molecules of SDS and N_{ct} of CTAB [9,10]. The scattering contrasts $\Delta\rho_s = \rho_s - \rho_w$ and $\Delta\rho_{ct} = \rho_{ct} - \rho_w$ are respectively the SLD differences of SDS and CTAB with respect to that of solvent ρ_w, which could be deduced [11] from the electron numbers of the surfactants and their partial specific volumes V_s (427 Å^3) [19] and V_{ct} (606 Å^3) [20] of SDS and CTAB, respectively, at 318 K. Therefore, N_s and N_{ct} of the ULV could be deduced model-independently [9-11], using two contrast values of X-ray $I_{o,X}(q=0)$ and neutron $I_{o,N}(q=0)$ of Eq. 3, in the absolute scattering intensity scales of units of cm^{-1} [15]:

$$N_s = (I_{o,X}/n_p)^{1/2}/(A_X+\chi B_X) \qquad (4)$$

$$N_{ct} = \chi N_s \quad (5)$$

with $\chi = (\mu A_N - A_X)/(\mu B_N - B_X)$ (6)

Here, $A_X = V_s\Delta\rho_{s\text{-}X}$, $A_N = V_s\Delta\rho_{s\text{-}N}$, $B_X = V_{ct}\Delta\rho_{ct\text{-}X}$, $B_N = V_{ct}\Delta\rho_{ct\text{-}N}$, and the square-root of the X-ray/neutron zero-angle scattering intensity ratio $\mu = \pm(I_{o,X}/I_{o,N})^{1/2}$. Assuming all CTAB form catanionic surfactant vesicles, the number density n_p may be approximated by the concentration C_{ct} of CTAB using $n_p = C_{ct}/N_{ct}$, neglecting the small CMC value of CTAB in the mixture. Previous studies showed that the critical aggregation concentrations of forming complex aggregates of SDS-CTAB were both below ca. 0.5 mM [21,22], which would be negligible in our study with the catanionic surfactant concentrations well above 10 mM. Even without accurate information of n_p, the association ratio of CTAB/SDS χ of the CS-ULV can still be deduced from Eq. 5 alone.

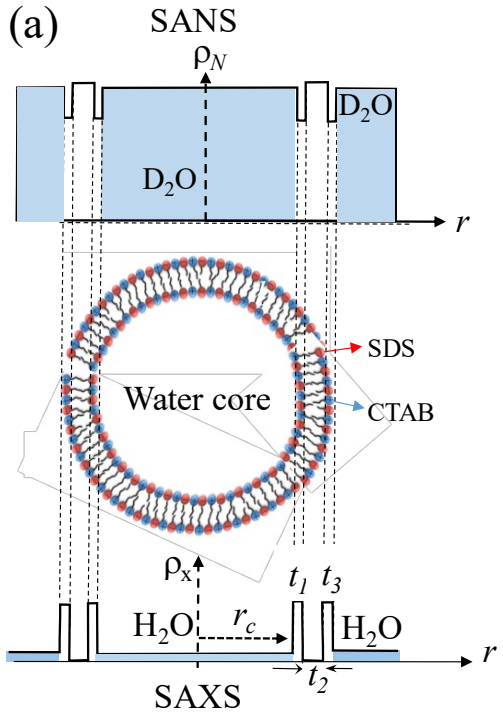

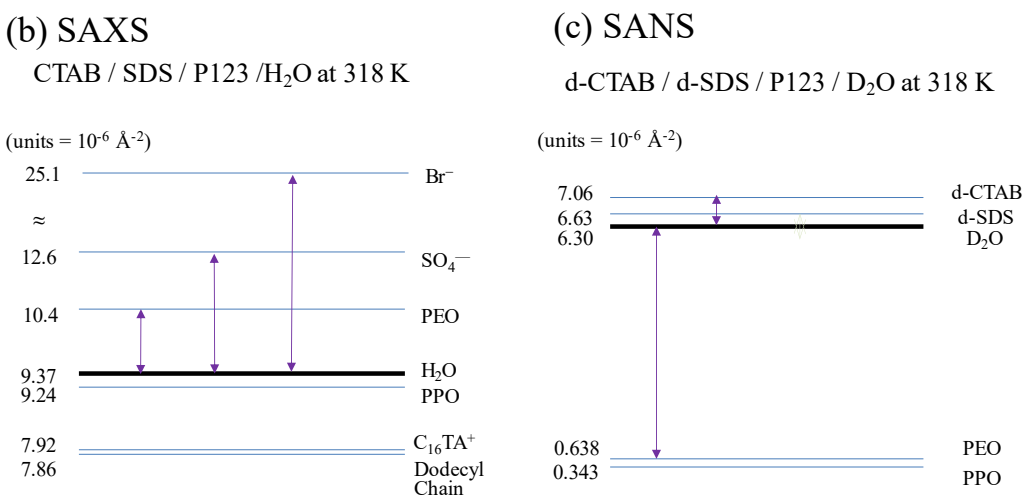

Fig. 1. (a) Neutron and X-ray SLD profiles, ρ_N (top) and ρ_x (bottom), for a simplified spherical core-shell-shell-shell model for the illustrated surfactant bilayer structure of the CS-ULV, with the central shell of deuterated aliphatic chains of SDS (d-SDS) and CTAB (d-CTAB); r_c is core radius of the CS-ULV, and $r_1 = r_c+t_1$ is the first shell radius comprising the hydrated headgroups of the catanionic surfactant. (b) The PO and EO groups are of ρ_x values of 9.24 and 10.4, and (c) ρ_N values of 0.343 and 0.638 and, in units of 10^{-6} Å^{-2}. Note that the central shell (t_2) of deuterated surfactant chains and D_2O core are of relatively high ρ_N values in SANS. By contrast, the two headgroup-shells are of high ρ_x values with respect to those for water and the surfactant chains in SAXS.

3. Results and discussion

3.1. CS-ULV structural features

Shown in Fig. 2a is the FFR-TEM image of the CS-ULV prepared from the solution of an SDS/CTAB ratio of R = 1.5, revealing globular particles of relatively uniform sizes of ca. 50 nm. Correspondingly, Fig. 2b are SAXS and SANS data measured for the CS-ULV sample solution. Both sets of data are characterized by a similar hump centered ca. q = 0.015 Å^{-1}, which corresponds to the core-size of CS-ULV of a few tens of nm. Further, the SAXS data exhibit a smeared semi-hump around 0.1 – 0.3 Å^{-1} and a hump centered at q ~ 0.4 Å^{-1}, which are features of a thin bilayer structure of the CS-ULV of a few nm. These features are, however,

less visible in the SANS data, due to the high incoherent background scattering in the relevant q-range. The SAXS and SANS data were jointly fitted with the shared geometrical parameters of r_c, t_1, t_2, and t_3 of the core-multi-shell $P(q)$ described previously, together with the same RMSA structure factor $S(q)$. The instrumental q-resolutions and neutron and X-ray scattering-lengths-densities (scattering contrast) of the corresponding sublayers were, however, fitted separately in the fitting algorithm. Such kind of joint fitting with shared geometrical parameters could effectively reduces overall fitting parameters and their fitting uncertainties, given a same amount of SAXS and SANS data. Inconsistent models from independent SAXS and SANS data fitting could also be avoided in the joint fitting algorithm in resolving complicated core-shell structures [23,24]. The methodology, however, assumes same solution structures in the sample solutions used for SAXS and SANS data collection. In our case, we used similar sample solutions and environmental conditions for SAXS and SANS, except that deuterated surfactants and D_2O were used in SANS, but not in SAXS. Nevertheless, a previous SANS study suggests that solvent isotope effects mainly affect the aggregation number but not the geometry of CTAB micelles [25]. Therefore, t_1, t_2, and t_3 of CS-ULV were fitted as common geometric parameters in our joint SANS-SAXS data fitting, as an approximation. The hence determined CS-ULV structural features include a core radius of r_c = 240±5 Å and a bilayer structure comprising a central shell of t_2 = 24±1 Å (corresponding to surfactant aliphatic chains) sandwiched by two thin shells of t_1 = t_3 = 4±1 Å thickness (surfactant headgroups). The overall bilayer thickness of 32 Å is consistent with that reported previously [6,26], and is significantly smaller than the tail-to-tail length of 41 Å or 49 Å of two SDS or CTAB molecules in all-trans conformation and serially aligned [26]. Presumably, the hydrophobic chains of the catanionic surfactant are highly interdigitated in the ULV bilayer.

The fitted structural parameters are summarized in Table 1.

We further calculate the two zero-angle intensities (in the absolute intensity scale of units of cm^{-1}) I_{oX} and I_{oN} from the fitted $P(q)$ profiles (Fig. 2b) of the SAXS and SANS data. From which two values, a CTAB/SDS composition ratio of 4:3 for the CS-ULV is deduced on the basis of Eq. (5). The composition ratio differs significantly from the overall solution CTAB/SDS molar ratio 2:3 (13.7 mM CTAB and 20.6 mM SDS). Such result may associate with the drastically lower CMC value 0.95 mM of CTAB, compared to that of SDS (CMC = 8.4 mM) [7,8]. Deducted with these CMC vales, the solution would form CS-ULV with ca. 12.6 mM of CTAB and 12.2 mM of SDS, which is comparable to the 4:3 ratio revealed from the SAXS and SANS results. We note that previous reports [21,22] indicated that SDS and CTAB could form aggregates at critical aggregation concentrations ca. 0.6 mM (below their CMC values). Nevertheless, when CTAB in the solution is exhausted in formation of largely neutralized aggregates of ULV with SDS, the excess SDS in solution might be subject to a similar CMC for formation of pure SDS micelles.

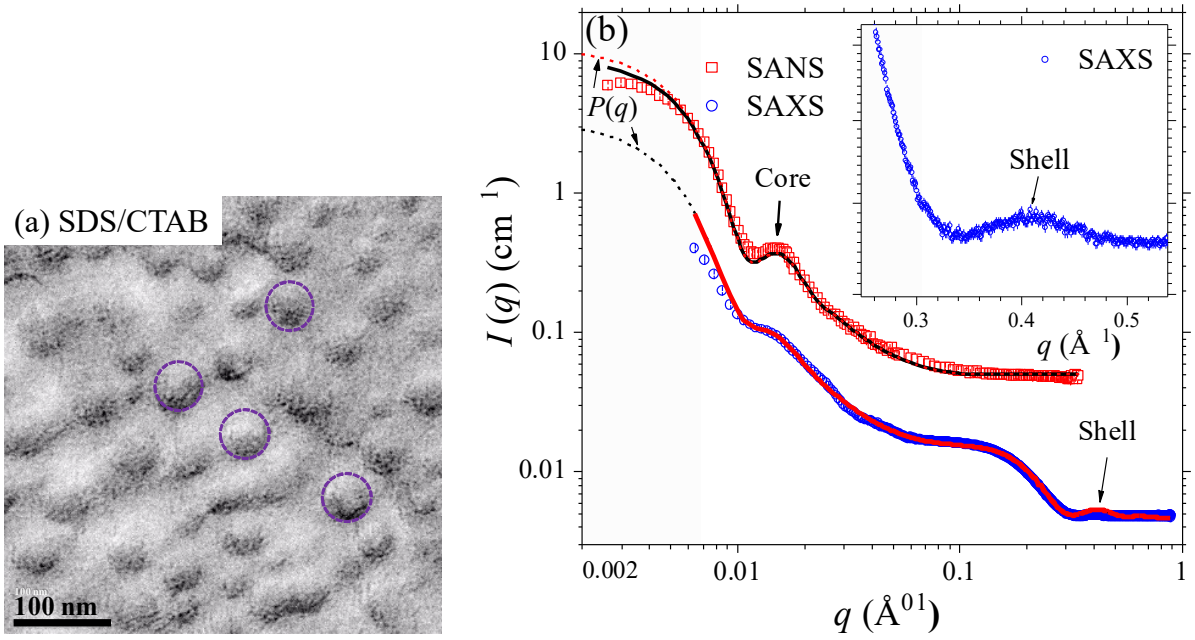

Fig. 2. (a) FFR-TEM image of the CS-ULV (selected circled) prepared from the solution of

SDS (20.6 mM) and CTAB (13.7 mM), showing globular particles of an average size ca. 50 nm. (b) Corresponding SANS and SAXS profiles of the CS-ULV solution, jointly fitted (solid curves) using the form factor (dotted curves) of core-multi-shell sphere (dotted curves) and the RMSA structure factor $S(q)$. The hump center around $q = 0.015$ Å^{-1} features the spherical core size of the CS-ULV, whereas as the SAXS high-q hump centered at 0.4 Å^{-1} (enlarged in the inset) associates with the bilayer shell structure.

Table 1. SANS-SAXS jointly fitted structural parameters using the core-multi-shell spherical model, together with a RMSA structure factor $S(q)$ of common parameters: the volume fraction 0.02 and charge number 52 of the CS-ULV and solution dielectric constant 78 and salt concentration 34 mM. The solvent SLD values used for SANS (D_2O) and SAXS data fitting are 6.30 and 9.37 in units of 10^{-6} Å^{-2}, at 318 K; t_1, t_2, and t_3 are shell thicknesses as indicated in Fig. 1a. Note that a polydispersity $p = 10\%$ in t_2 and a pinhole smearing of 2% for the data q-resolution were used in the data fitting.

Parameters	SANS	SAXS
ρ_1 (10^{-6} Å^{-2})	4.35±0.02	13.59±0.05
ρ_2 (10^{-6} Å^{-2})	6.31±0.05	7.43±0.03
ρ_3 (10^{-6} Å^{-2})	4.35±0.02	13.59±0.05
r_c (Å)	240±5	
p (%) in r_c	25±4	
t_1 (Å)	4.1±0.1	
t_2 (Å)	23.8±0.4	
t_3 (Å)	4.1±0.1	

3.2. P123-embedded CS-ULV

Fig. 3a-d shows the FFR-TEM images of the CS-ULV (selectively circled) in solutions of 20.6 mM SDS and 13.7 mM CTAB, added with different P123 concentrations x. These images reveal increased sizes of the CS-ULV upon addition of P123; in addition, an enlarged mean hydrodynamic diameter of P123-embedded CS-ULV in solution added with 0.04 mM P123, compared to the neat CS-ULV, is consistently observed using dynamic light scattering (DLS) (Fig. 3e). Presumably, P123 could intervene into the CS-ULV bilayer for enlarged vesicle sizes. We notice that above 0.08 mM P123, particles of ~20 nm start to appear, and proliferate with further increase of P123 concentration (Fig. 3c-d). These aggregates are attributed to P123-

based core-shell micelles, according to a previous report [11].

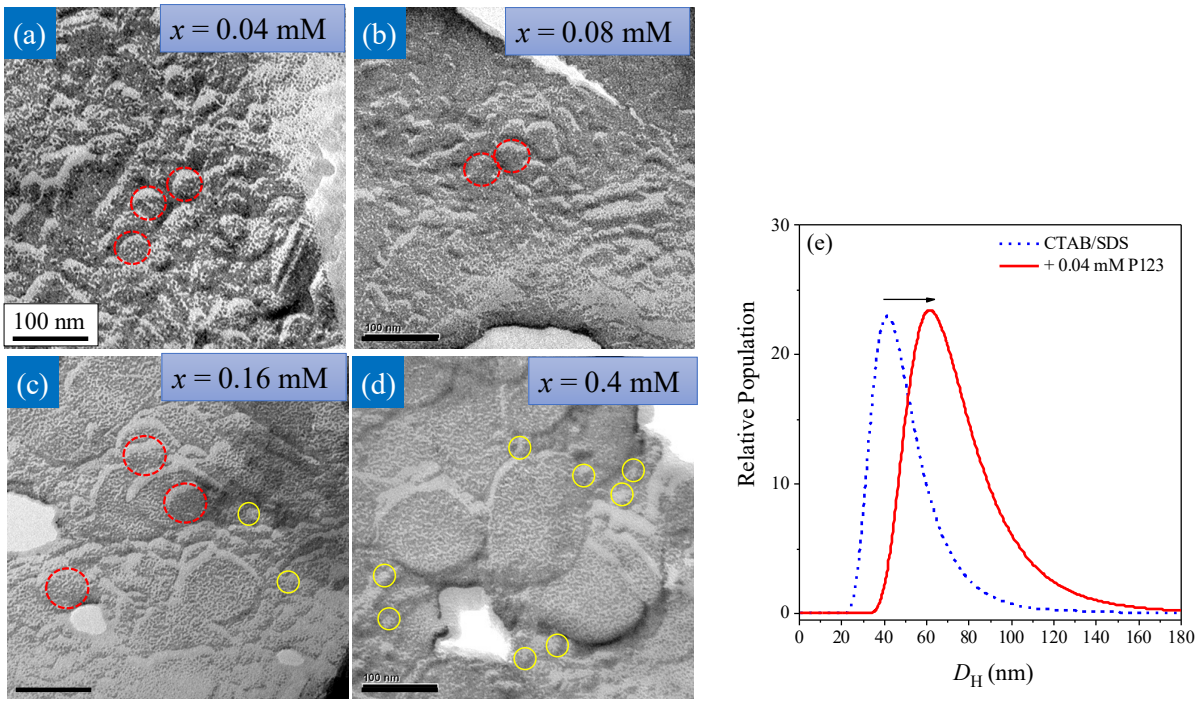

Fig. 3. FFR-TEM images of the CS-ULV (selected circled) in solutions of 20.6 mM SDS and 13.7 mM CTAB, added with P123 of concentrations *x* of (a) 0.04 mM, (b) 0.08 mM, (c) 0.16 mM, and (d), 0.4 mM. Selectively dotted circled in red in (a)-(c) are slightly enlarged CS-ULV with increase of P123 concentrations. The globular shape and size are mainly outlined by the 2-nm coating layer of platinum-carbon of high electron density. Selectively circled in yellow in (c)-(d) are relatively small (~20 nm) P123-based micelles. Note that the large flat disks (~200 nm) are attributed to aggregates of the P123-based micelles [11]. The scaling bar represents 100 nm. (e) DLS-determined distribution of the hydrodynamic diameter D_H of the neat CS-ULV without P123, compared to that added with 0.04 mM P123.

The corresponding sets of SANS data for the CS-ULV solutions with successively increased P123 concentrations are shown in Fig. 4a. The characteristic core-size hump of CS-ULV shifts systematically toward the lower *q*-region from that (0.015 $Å^{-1}$) of neat CS-ULV, revealing consistently increased core sizes of P123-embedded CS-ULV with solution P123 concentration, which are consistent with that observed in the FFR-TEM images (Fig. 3). Fig. 4a also reveals that,

over ~0.08 mM of P123, the SANS intensity in the q-range of 0.02 – 0.1 $Å^{-1}$ enhances roughly linearly with the P123 concentration. The result suggests that increasingly more excessed P123 (presumably excluded from the CS-ULV) could form P123-based micelles. Due to the high scattering contrast of the P123 micelles with respect to the solvent D_2O, formation and proliferation of P123 core-shell micelles of similar sizes in the solution are better revealed in the SANS data, but not in the parallel SAXS data (Fig. 4b). Therefore, we assign the intensity increase in this region mainly to P123-based core-shell micelles. SANS data for higher P123 concentrations of 0.4, 0.8, and 1.6 mM P123 were taken mainly for extrapolating the critical aggregation concentration of P123-based micelles as detailed below in Fig. 5. The parallel SAXS data with 0.4, 0.8, and 1.6 mM P123 were, however, neglected as they would not contribute more information of the CS-ULV/P123 complex.

Using the same SANS-SAXS joint-fitting algorithm as that used for the pure CS-ULV case, we fitted the parallel sets of the SANS and SAXS data in Fig. 4 using (*i*) the core-multi-shell spheres with an RMSA structure factor for the P123-embeddd CS-ULV and (*ii*) core-shell prolate P123-based micelles (with an RMSA structure factor included for the solutions of higher P123 concentrations) [11]. We note that the bilayer structural parameters t_1, t_2, and t_3 are jointly fitted with the parallel SAXS and SANS data sets for consistency and reduced fitting parameters. The structure factors used for these charged aggregates were found to be insensitive in the data fitting (cf. the small volume fractions summarized in Table 2); the use of $S(q)$, however, improves slightly the fitting quality in the low-q region. All the fitted parameters for the complementary SANS and SAXS data sets are summarized in Table 2; which indicates similar SLD values and shell structures (t_1, t_2, and t_3) for the CS-ULV-P123 complex in the solutions of 0.04 - 0.16 mM of P123 (cf. Table 2). The fitting results reveal a relative stable vesicle bilayer structure of the CS-ULV/P123

complex; the core size r_c, hence the overall CS-ULV size, increases with the P123 concentration. From the fitted SLD values of the CS-ULV/P123 complex (Table 2) and the corresponding values of the neat CS-ULV (Table 1), we could deduce a 3% volume fraction of the PPO blocks of P123 in the t_2 layer, on the basis of the individual SLD values of the relevant components shown in Fig. 1. The very thin t_3 layer of a few Å thickness involves the head groups of the surfactants, water molecules, and the PEO blocks of P123. Therefore, an additional set of contrast-varied data would be needed to resolve the PEO volume fraction in the three-phase t_3 layer.

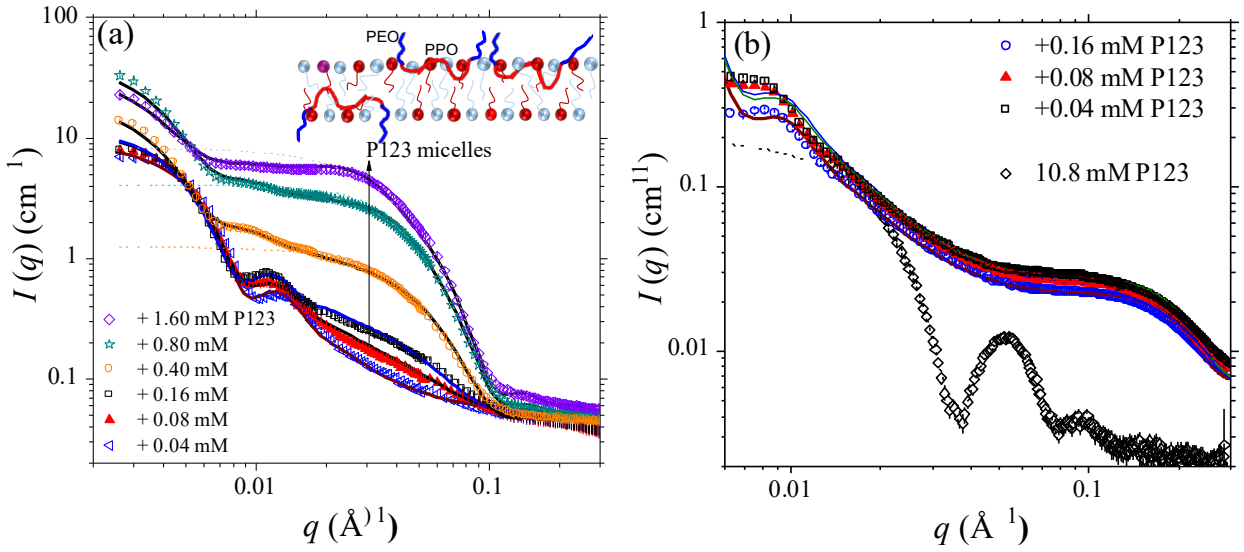

Fig. 4. (a) SANS and (b) SAXS data of the CS-ULV solutions of SDS/CTAB, with successively increased P123 concentrations. The SANS data are fitted (solid curves) using (*i*) a core-multi-shell sphere model with a RMSA structure factor for P123-embedded CS-ULV, together with (*ii*) an prolate core-shell form factor (accompanied by a RMSA structure factor when P123 concentration is above 0.16 mM) for the P123-based micelles (dotted curves). A model of P123-embedded ULV bilayer of SDS-CTAB (with red and sky-blue balls for the headgroups) is shown in the inset in (a). The low and insensitive SAXS contribution of P123-based micelles is neglected in the SAXS data fitting. Also shown is the low scattering intensity profile of neat P123 micelles in a solution of 10.8 mM P123, which data are fitted (dotted curve) with core-shell spheres of a core radius of 60.4 Å and a shell thickness of 36.5 Å.

Table 2. SANS-SAXS jointly fitted structural parameters for the fitting curves in Fig. 4, using (*i*) the core-multi-shell spheres with an RMSA structure factor $S(q)$ (of volume fraction η and effective diameter σ), with fixed charge number 52 (insensitive), dielectric constant 78, and salt concentration 34 mM, at 318 K, and (*ii*) the core-shell prolate (added with an RMSA

structure factor $S(q)$ when the P123 concentration is above 0.16 mM). The parameters t_1, t_2, and t_3 are shell thicknesses of CS-ULV as indicated in Fig. 1a. a_c and b_c are the semi-major and semi-minor axes of the PO-core (with SLD $\rho_{c\text{-}PO}$) of the P123-based micelles, whereas a and b are that of the overall prolate micelle, including the PEO-shell (with SLD $\rho_{c\text{-}EO}$). The solvent SLD values used in SANS (D_2O) and SAXS data fitting are 6.30 and 9.37 in units of 10^{-6} Å^{-2}, at 318 K. Parameters fixed in the data fitting are marked by *.

SANS: CS-ULV						
P123 Concentration	0.04 mM	0.08 mM	0.16 mM	0.4 mM	0.8 mM	1.6 mM
ρ_1 (10^{-6} Å^{-2})	5.30±0.01	5.31±0.01	5.31±0.01	5.30*	5.30*	5.30*
ρ_2 (10^{-6} Å^{-2})	6.12±0.30	6.15±0.10	6.11±0.10	6.12*	6.12*	6.12*
ρ_3 (10^{-6} Å^{-2})	5.30±0.01	5.31±0.01	5.31±0.01	5.30*	5.30*	5.30*
r_c (Å)	297±2	319±3	342±5	398±4	402±4	410±5
p(%) in r_c	19	20	15	25	25	26
t_1 (Å)	4.7±0.1	4.8±0.1	4.8±0.1	4.7±0.1	4.7*	4.7*
t_2 (Å)	24.5±0.1	24.3±0.1	24.3±0.1	24.5±0.1	24.5*	24.5*
t_3 (Å)	4.7±0.1	4.8±0.1	4.8±0.1	4.7±0.1	4.7*	4.7*
SANS: P123 Prolate Core-Shell Micelles						
*$\rho_{c\text{-}PO}$ (10^{-6} Å^{-2})	-	0.343	0.343	0.343	0.343	0.343
$\rho_{s\text{-}EO}$ (10^{-6} Å^{-2})	-	2.37*	2.37*	2.37±0.05	2.32±0.05	2.32±0.05
a_c (Å)	-	48.9*	48.9*	63.2±0.3	77.8±0.2	84.7±0.2
b_c (Å)	-	30.6*	30.6*	30.1±0.2	31.1±0.1	33.1±0.1
a (Å)	-	66.2*	66.2*	72.2±0.5	88.3±0.5	97.4±0.3
b (Å)	-	36.3*	36.3*	36.1±0.3	38.1±0.2	39.0±0.2
η	-	-	-	0.032	0.049	0.070
σ (Å)	-	-	-	38.5	50.5	95.9
SAXS: CS-ULV						
P123 Concentration	0.04 mM	0.08 mM	0.16 mM			
ρ_1 (10^{-6} Å^{-2})	13.01±0.01	12.90±0.01	13.06±0.04			
ρ_2 (10^{-6} Å^{-2})	7.49±0.02	7.50±0.03	7.47±0.02			
ρ_3 (10^{-6} Å^{-2})	13.01±0.01	12.90±0.01	13.06±0.04			
r_c (Å)	388±3	394±3	394±5			
p(%) in r_c	24	24	24			

Interestingly, structural parameters in Table 2 indicate that the bilayer thicknesses fitted for the P123-embedded CS-ULV in the solutions of different P123 concentrations maintains a similar size of 34 Å (with similar hydrophobic and hydrophilic shell thicknesses), which is only marginally larger than that (32 Å) of the neat CS-ULV. These features would suggest that P123 may intervene into the CS-ULV bilayer with highly extended PPO chains confined within the

hydrophobic surfactant-tail layer of the CS-ULV; correspondingly, the PEO chains may extend away from the CS-ULV bilayers and into the solution (hence affecting little the headgroup shell thickness of the CS-ULV), as illustrated in the inset of Fig. 4a. With the proposed model, the P123-embedded CS-ULV bilayer would have an enhanced bending constant due to locally coordinated (bundled) catanionic surfactant via networking of the PPO chains of P123. The larger bending constant consequently would facilitate stabilizing the bilayer structure for the enlarged vesicle sizes observed, as suggested in a previous report [27]. Previously, hydrophobic styrene was also shown to incorporate into the hydrophobic shell of a similar CS-ULV bilayer for increased vesicle sizes; there, the bilayer thickness of the styrene-loaded ULV was also found to maintain largely constant [28].

Furthermore, the corresponding SANS zero-angle intensities contributed solely from the P123-based micelles (Fig. 4a) are calculated using the fitted form factor, and correlated to the P123 concentration in solution, as shown in Fig. 5; the intensity growth can be fitted with a linear relationship, with an intercept of zero-intensity of 0.067±0.008 mM. Which value corresponds to a critical aggregation concentration (CAC) for formation of P123-based micelles in the CS-ULV solution [8,11]. The CAC value may be regarded as an upper limit of P123-carrying capacity of the CS-ULV. Assuming that most of 13.7 mM CTAB and 0.067 mM P123 (CAC) in the solution form the CS-ULV, we could deduce a molecular ratio ca. 1:200 of P123:CTAB for the catanionic CS-ULV. We note that the CMC of P123 in aqueous solution at 318 K was reported to be vanishingly small [13].

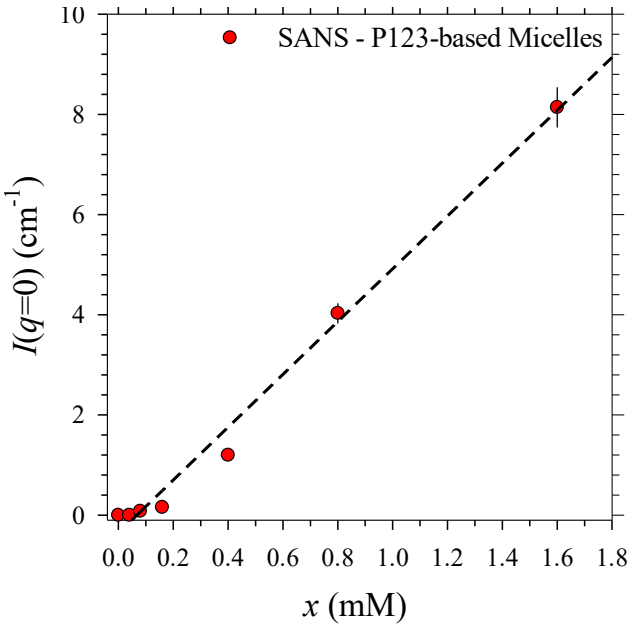

Fig. 5. Deconvoluted SANS intensities contributed solely by the P123 prolate core-shell micelles in the solutions of 20.6 mM SDS and 13.7 mM CTAB, added with different P123 concentrations x. The data are linearly fitted (dotted line) with a zero-intensity intercept of 0.067±0.008 mM P123.

4. Conclusions

We have elucidated the bilayer structure and composition of the catanionic unilamellar vesicles formed in the solution of CTAB and SDS, using complementary SAXS and SANS and supplementary FFR-TEM. The observed 50-nm CS-ULV is of a bilayer thickness of 32 Å and a composition ratio of CTAB/SDS = 4:3. Triblock copolymer P123 is suggested to intervene into the CS-ULV bilayer, leading to enlarged core sizes of the CS-ULV and slightly increased bilayer thickness of 34 Å. A P123-carrying capacity of the catanionic ULV is estimated to be P123:CTAB ~ 1:200, in solutions of SDS and CTAB (molar ratio 1.5:1) concentrations well above their CMC values. The P123-embedded CS-ULV bilayers have two nice features for future applications in drug carrying, including (a) the better stabilized bilayer structure for enlarged vesicle sizes under challenging conditions encountered in drug loading or delivering and (b) the protruding PEO groups of P123 on the interfaces of CS-ULV, which may naturally serve the necessary stealth

function of a good drug carrier, just like the PEGylation in liposome. We are aware that CTAB of the catanionic surfactant used in this work may not be a good candidate in drug formulation because of its cytotoxicity. However, the detailed structural knowledge obtained on the complex vesicles from mixtures of the catanionic and pluronic type polymer broadens the scope of new types of vesicle carriers.

Declaration of competing interest The authors declare that they have no known competing financial interests or personal relationships that could have appeared to influence the work reported in this paper. The authors declare that they have no conflict of interest.

Acknowledgement.

We thank Drs. Z. Di and H. Frielinghaus for assistance in SANS data collection. This work benefited from the use of the SasView application, originally developed under NSF award DMR-0520547. SasView contains code developed with funding from the European Union's Horizon 2020 research and innovation programme under the SINE2020 project, grant agreement No 654000. Funding supports from Ministry of Science and Technology of Taiwan (110-2811-M-213-509 and 109-2811-M-213-500) and program of user cultivation of Taiwan neutron facility (under the proposal 2009-2-074-4 of NSRRC) are acknowledged.

References

1. G. Milcovich, F. E. Antunes, M. Grassi, F. Asaro, Stabilization of unilamellar catanionic vesicles induced by β-cyclodextrins: A strategy for a tunable drug delivery depot, Int. J. Pharma. 548 (2018) 474–479.

2. S. Rajkhowa, S. Mahiuddin, J. Dey, S. Kumar, V. K. Aswal, R. Biswas, J. Kohlbrechere, K. Ismail, The effect of temperature, composition and alcohols on the microstructures of catanionic mixtures of sodium dodecylsulfate and cetyltrimethylammonium bromide in water Soft Matter, 13 (2017) 3556-3567.
3. S. Geng, Y. Wang, L. Wang, T. Kouyama, T. Gotoh, S. Wada, J.-Y. Wang, A Light-Responsive Self-Assembly Formed by a Cationic Azobenzene Derivative and SDS as a Drug Delivery System, Sci. Rep. 7 (2017) 39202-13.
4. J. N. Israelachvili, Intermolecular and Surface Forces, Academic Press, London, 1992.
5. V. Tomasic, I. Stefanic, N. Filipovic-Vincekovic, Adsorption, association and precipitation in hexadecyltrimethylammonium bromide/sodium dodecyl sulfate mixtures Colloid. Polym. Sci. 277 (1999) 153-163.
6. P. Andreozzi, S. S. Funari, C. La Mesa, P. Mariani, M. G. Ortore, R. Sinibaldi, F. Spinozzi, Multi- to Unilamellar Transitions in Catanionic Vesicles, J. Phys. Chem. B, 114 (2010) 8056–8060
7. A. Mal, S. Bag, S. Ghosh, S. P. Moulik, Physicochemistry of CTAB-SDS interacted catanionic micelle-vesicle forming system: An extended exploration, Colloid. Surf. A: Physi. Engi. Asp. 553 (2018) 633-644.
8. B. Sohrabi, H. Gharibi, B. Tajik, S. Javadian, M. Hashemianzadeh, Molecular Interactions of Cationic and Anionic Surfactants in Mixed Monolayers and Aggregates J. Phys. Chem. B, 112 (2008) 14869–14876.
9. U. Jeng, T.-L. Lin, C.-S. Tsao, C.-H. Lee, L. Y. Wang, L. Y. Chiang, C. C. Han, Study of Aggregates of Fullerene-Based Ionomers in Aqueous Solutions Using Small Angle Neutron and X-ray Scattering, J. Phys. Chem. B, 103 (1999) 1059-1063.

10. J.-M. Lin, T.-L. Lin, U. Jeng, Z.-H. Huang, Y.-S. Huang, Aggregation Structure of Alzheimer Amyloid-beta(1-40) Peptide with Sodium Dodecyl Sulfate as Revealed by Small-angle X-ray and Neutron Scattering, Soft Matter, 5 (2009) 3913–3919.
11. Y.-Q. Yeh, C.-J. Su, C.-A. Wang, Y.-C. Lai, C.-Y. Tang, Z. Di, H. Frielinghaus, A.-C. Su, U. Jeng, C.-Y. Mou, Diatom-inspired self-assembly for silica thin sheets of perpendicular nanochannels, J. Colloid. Interf. Sci. 584 (2021) 647–659.
12. E. Soussan, S. Cassel, M. Blanzat, I. Rico-Lattes, Drug Delivery by Soft Matter: Matrix and Vesicular Carriers, Angew. Chem. Int. Ed. 48 (2009) 274 – 288.
13. P. Alexandridis, J. F. Holzwarth, T. A. Hatton, Micellization of Polyethylene oxide)-Poly(propylene oxide)-Poly(ethylene oxide) Triblock Copolymers in Aqueous Solutions: Thermodynamics of Copolymer Association, Macromolecules 27 (1994) 2414-2425.
14. B. Jacrot, The study of biological structures by neutron scattering from solution. Rep. Prog. Phys. 39 (1976) 911-953.
15. U. Jeng, C.-H. Su, C.-J. Su, K.-F. Liao, W.-T. Chuang, Y.-H. Lai, Y.-J. Chang, Y.-J. Chen, Y.-S. Huang, M.-T. Lee, K.-L. Yu, J.-M. Lin, D.-G. Liu, C.-F. Chang, C.-Y. Liu, C.-H. Chang, K. S. Liang, A small/wide-angle X-ray scattering instrument for structural characterization of air-liquid interfaces, thin films, and bulk specimens, J. Appl. Cryst. 43 (2010) 110-121.
16. A.V. Feoktystov, H. Frielinghaus, Z. Di, S. Jaksch, V. Pipich, M.-S. Appavou, E. Babcock, R. Hanslik, R. Engels, G. Kemmerling, H. Kleines, A. Ioffe, D. Richter, T. Brückel, A.V. Feoktystov, H. Frielinghaus, Z. Di, S. Jaksch, V. Pipich, M.-S. Appavou, E. Babcock, R. Hanslik, R. Engels, G. Kemmerling, H. Kleines, A. Ioffe, D. Richter, T. Brückel, J. Appl. Cryst. 48 (2015) 61-70, J. Appl. Cryst. 48 (2015) 61-70.

17. J. B. Hayter, J. Penfold, Determination of micelle structure and charge by neutron small-angle Scattering, Colloid Polym. Sci. 261 (1983) 1022-1030.
18. M. Kotlarchyk, S.-H. Chen, Analysis of small angle neutron scattering spectra from polydisperse interacting colloids, J. Chem. Phys., 79 (1983) 2461-2469.
19. P. C. Griffiths, A. Paul, R. K. Heenan, J. Penfold, R. Radha, B. L. Bales, Role of Counterion Concentration in Determining Micelle Aggregation: Evaluation of the Combination of Constraints from Small-Angle Neutron Scattering, Electron Paramagnetic Resonance, and Time-Resolved Fluorescence Quenching, J. Phys. Chem. B 108 (2004) 3810-3816
20. A. Heins, V.M. Garamus, B. Steffen, H. Stöckmann, K. Schwarz, Impact of phenolic antioxidants on structural properties of micellar solutions, Food Biophys. 1 (2006) 189–201.
21. A. Mal, S. Ghosh, S. P. Moulik, Time dependent physicochemical changes of SDS-CTAB interacted self assembled vesicles: Ostwald ripening effect, Colloids Surf. A: Physicochem. Eng. Asp. 617 (2021), 126328-122.
22. S. B. Lioi, X. Wang, M. R. Islam, E. J. Danoff, D. S. English, Catanionic surfactant vesicles for electrostatic molecular sequestration and separation, Phys. Chem. Chem. Phys. 11 (2009) 9315-9325.
23. M. J. Hollamby, K. Aratsu, B. R. Pauw, S. E. Rogers, A. J. Smith, M. Yamauchi, X. Lin, S. Yagai, Simultaneous SAXS and SANS analysis for the detection of toroidal supramolecular polymers composed of noncovalent supermacrocycles in solution, Angew. Chem. Int. Ed., 55 (2016) 9890-9893.
24. B. Eicher, F. A. Heberle, D. Marquardt, G. N. Rechberger, J. Katsaras, G. Pabst, Joint SAXS/SANS data analysis of asymmetric lipid vesicles, J. Appl. Cryst. 50 (2017) 419-429.
25. S. S. Berrt, Solvent isotope effects on alkyltrlmethylammonlum bromide micelles as a function of alkyl chain length, J. Phys. Chem. 91 (1987) 4760-4765.

26. I. R. Krauss, R. Imperatore, A. De Santis, A. Luchini, Structure and dynamics of cetyltrimethylammonium chloride-sodium dodecylsulfate (CTAC-SDS) catanionic vesicles: High-value nano-vehicles from low-cost surfactants J. Colloid Interf. Sci, 501 (2017) 112–122.
27. L. Paduano, G. D'Errico, H. T. Jung, B. Coldren, J. A. Zasadzinski, D. J. Iampietro, E. W. Kaler, The origins of stability of spontaneous vesicles, Proc. Natl. Acad. Sci. USA, 98 (2001) 1353–1357.
28. H. Yalcinkaya, K. Bressel, P. Lindner, M. Gradzielski, Controlled formation of vesicles with added styrene and their fixation by polymerization, J. Colloid. Interf. Sci. 531 (2018) 672–680.